



LAWRENCE
LIVERMORE
NATIONAL
LABORATORY

Solid-Phase Isotope Harvesting of ^{88}Zr from a Radioactive Ion Beam Facility

J. Bence, S. Satija, K. A. Domnanich, J. D. Despotopoulos, E.
P. Abel, H. K. Clause, S. Essenmacher, C. Kalman, C.
Kleinfeldt, K. N. Kmak, T. Parsons-Davis, C. Vyas, W. Walker,
N. D. Scielzo, G. W. Severin, J. A. Shusterman

March 4, 2022

Applied Radiation and Isotopes

Disclaimer

This document was prepared as an account of work sponsored by an agency of the United States government. Neither the United States government nor Lawrence Livermore National Security, LLC, nor any of their employees makes any warranty, expressed or implied, or assumes any legal liability or responsibility for the accuracy, completeness, or usefulness of any information, apparatus, product, or process disclosed, or represents that its use would not infringe privately owned rights. Reference herein to any specific commercial product, process, or service by trade name, trademark, manufacturer, or otherwise does not necessarily constitute or imply its endorsement, recommendation, or favoring by the United States government or Lawrence Livermore National Security, LLC. The views and opinions of authors expressed herein do not necessarily state or reflect those of the United States government or Lawrence Livermore National Security, LLC, and shall not be used for advertising or product endorsement purposes.

Solid-Phase Isotope Harvesting of ^{88}Zr from a Radioactive Ion Beam Facility

Jake A. Bence,^{1,2} Samridhi Satija,^{3,4} Katharina A. Domnanich,^{3,4} John D. Despotopoulos,⁵ E. Paige Abel,^{3,4} Hannah K. Clause,^{3,4} Scott Essenmacher,^{3,4} Morgan Kalman,^{3,4} Chloe Kleinfeldt,^{3,4} Kelly N. Kmak,⁵ Tashi Parsons-Davis,⁵ Chirag K. Vyas,^{3,4} Wesley Walker,^{3,4} Nicholas D. Scielzo,⁵ Gregory W. Severin,^{3,4} and Jennifer A. Shusterman,^{1,2,5*}

¹ Hunter College of the City University of New York, New York, New York 10065, USA

² Graduate Center of the City University of New York, New York, New York 10016, USA

³ Department of Chemistry, Michigan State University, East Lansing, Michigan 48824, USA

⁴ Facility for Rare Isotope Beams, Michigan State University, East Lansing, Michigan 48824, USA

⁵ Lawrence Livermore National Laboratory, Livermore, California 94550, USA

*Corresponding Author

Abstract

During routine operation of the Facility for Rare Isotope Beams (FRIB), radionuclides will accumulate in both the aqueous beam dump and along the beamline in the process of beam purification. These byproduct radionuclides, many of which are far from stability, can be collected and purified for use in other scientific applications in a process called isotope harvesting. In this work, the viability of ^{88}Zr harvesting from solid components was investigated at the National Superconducting Cyclotron Laboratory. A secondary ^{88}Zr beam was stopped in a series of collectors comprised of Al, Cu, W, and Au foils. This work details irradiation of the collector foils and the subsequent radiochemical processing to isolate the deposited ^{88}Zr (and its daughter ^{88}Y) from them. Total average recovery from the Al, Cu, and Au collector foils was $(91.3 \pm 8.9) \%$ for ^{88}Zr and $(95.0 \pm 5.8) \%$ for ^{88}Y , respectively, which is over three times higher recovery than in a previous aqueous-phase harvesting experiment. The utility of solid-phase isotope harvesting to access elements such as Zr that readily hydrolyze in near-neutral pH aqueous conditions has been demonstrated for application to harvesting from solid components at FRIB.

1. Introduction

Radioactive ion beam (RIB) facilities are user facilities that accelerate beams of nuclides for nuclear science research, especially for studying rare isotopes. The National Superconducting Cyclotron Laboratory (NSCL) and its successor, the Facility for Rare Isotope Beams (FRIB) at Michigan State University (MSU), produce RIBs through the fragmentation of heavy ions accelerated into a light production target. The resulting fragmentation products are transferred to an in-flight mass separator to select the desired secondary ions from the primary beam to be delivered to the user experiment. Through this process, a broad distribution of fragmentation products will accumulate at various points within the accelerator. Approximately 90% of the initial primary beam remains unreacted and will be deposited into the aqueous beam dump, which is designed to capture the excess beam fragments for potential reuse. (Abel et al., 2019; Domnanich et al., 2020a) Beam products will accumulate at the beam dump, beam stops, and collimators, among other points. The process of collecting and purifying these byproduct radionuclides for other uses without interruption of the user experiment has been termed 'isotope harvesting'. FRIB will produce a wider variety and greater quantity of radionuclides than

the NSCL, offering the potential for an unprecedented supply of exotic radionuclides via isotope harvesting.

Typical radionuclide production routes involve dedicated irradiations of target material with charged particles at a cyclotron or linear accelerator, or with neutrons at a nuclear reactor. Isotope harvesting at FRIB, however, is a means of production that will occur as a byproduct of other primary user experiments at the facility. FRIB is unique in its incorporation of isotope-harvesting facilities from initial construction; all other RIB facilities have retrofitted the capability to extract radionuclides from existing systems. For example, the Exotic Radionuclides from Accelerator Waste for Science and Technology (ERAWAST) initiative at the Paul Scherrer Institute (PSI), separated long-lived radionuclides from previously irradiated materials. (Schumann et al., 2013b) Example radionuclides include ^{44}Ti from steel, (Margerin et al., 2014) ^7Be from cooling water, (Schumann et al., 2013a) and ^6Al , ^{59}Ni , ^{44}Ti , ^{53}Mn and ^{60}Fe from a proton-irradiated copper beam dump. (Ayranov and Schumann, 2010) From tantalum and tungsten targets irradiated at the SATURNE II synchrotron of the Laboratoire National Saturne (LNS) at Saclay, ^{36}Cl , ^{129}I , ^{146}Sm , ^{148}Gd , ^{150}Gd (only from tantalum) and ^{154}Dy have been separated. (Talip et al., 2021, 2017) The purified radionuclides were subsequently used for a variety of applications ranging from nuclear-data measurements to radiopharmaceutical studies.

Preliminary isotope harvesting efforts with aqueous matrices (aqueous-phase isotope harvesting) have been performed at the NSCL to prepare for harvesting from the aqueous beam dump at FRIB. To date, these experiments have targeted ^{24}Na , (Pen et al., 2014) $^{47}\text{Ca}/^{47}\text{Sc}$, (Abel et al., 2020) ^{48}V , (Loveless et al., 2020) ^{62}Zn , (Domnanich et al., 2020b) ^{67}Cu , (Mastren et al., 2015, 2014) and ^{88}Zr . (Shusterman et al., 2021) Aqueous-phase isotope harvesting experiments conducted on ^{88}Zr and ^{48}V in near-neutral pH resulted in lower recovery yields than those of the other reported radionuclides. (Loveless et al., 2020; Shusterman et al., 2021) Group IV and V elements, including Zr and V, tend to exhibit multiple oxidation states, complex speciation chemistry, and propensity to hydrolyze in aqueous solution, even in acidic matrices. These properties make harvesting isotopes of these elements from near-neutral pH aqueous environments more challenging. (Fritz and Abbink, 1962) For example, V can exist in either cationic or anionic forms in near-neutral pH ranges. (Fritz and Abbink, 1962; Takeno, 2005) Zr readily hydrolyzes, forming inert hydroxide and oxyhydroxide complexes when in aqueous solutions. (Connick and McVey, 1949; Dewell and Voight, 1951; Ellis P. Steinberg, 1960; Kraus and Johnson, 1953) Low recovery yields for Zr and V are likely due to their speciation chemistry, motivating this work on solid-phase isotope harvesting which avoids near-neutral pH aqueous conditions. Solid-phase isotope harvesting is the process of recovering desirable beam fragmentation products from solid materials. It can be implemented in parallel to user experiments and aqueous-phase isotope harvesting at the beam dump.

Zr has several radioisotopes of interest in nuclear science, such as ^{89}Zr in positron emission tomography (PET), (Deri et al., 2013) ^{86}Zr as the radioactive parent to the PET isotope ^{86}Y , (Baimukhanova et al., 2018) and ^{95}Zr as an s-process branch-point nucleus. (Sonnabend et al., 2003) ^{88}Zr ($t_{1/2} = 83.4$ days) is relevant for interpreting historic nuclear test data for stockpile stewardship, and it can be used as a tracer for studying Zr chemistry due to its suitable half-life and characteristic γ -ray emission. (Hoffman et al., 2006; Reis et al., 2016) ^{88}Zr is a neutron-deficient isotope that decays by electron capture to ^{88}Y ($t_{1/2} = 106.63$ days) and emits an intense 393 keV γ -ray ($I = 97\%$). (McCutchan and Sonzogni, 2014) Recently, ^{88}Zr was discovered to have one of the highest neutron-capture cross-sections ever measured. (Shusterman et al., 2019) Like the majority of radioactive nuclei, there are limited cross-section data on ^{88}Zr due in part to the difficulty in obtaining enough pure target material for a reliable measurement. Isotope

harvesting can provide a pathway to access radioactive nuclei that are otherwise difficult to produce, allowing for fabrication of radioactive target materials for subsequent nuclear-data measurements.

The solid collector foils used in this work were Al, Cu, W, and Au, chosen to represent solid beamline materials that may accumulate byproduct radionuclides during routine operations at FRIB, or that may be desirable for implementation as fragment catchers. For example, Al is commonly used for solid components due to its high durability, low density, and low cost. Cu is useful for its ductility and both thermal and electrical conductivity. W is dense and has a high melting point, thus typically used for radiation shielding or beam stops in nuclear science experiments.¹ Au can be rapidly dissolved and separated from many other elements because of its unique chemistry, making it a promising material for a fragment catcher for short-lived radionuclides. By dissolving each of these collectors in highly acidic matrices prior to radiochemical separation, hydrolyzing conditions are avoided, ideally improving Zr recovery yields. The previous aqueous-phase isotope harvesting experiment of ⁸⁸Zr reported a total recovery of (26 ± 2) % of ⁸⁸Zr deposited into an aqueous target. (Shusterman et al., 2021) In this work, solid-phase isotope harvesting of ⁸⁸Zr is investigated for a direct comparison to the aqueous-phase isotope harvesting study. The solid-phase isotope harvesting methods described below provide a methodology for collection of ⁸⁸Zr which can subsequently be applied to group IV and other elements with complex aqueous chemistry.

2. Experimental

2.1. *Materials and supplies*

The Al (99.45%, 0.025 mm thick, Alfa Aesar), Cu (99.8%, 0.025 mm thick, Alfa Aesar), W (99.95%, 0.05 mm thick, Alfa Aesar), and Au (99.95 %, 0.025 mm thick, Goodfellow) foils were all cut into a circle with a diameter of 2.54 cm, cleaned with isopropanol (99.99%, Fisher), and scored to label before loading into the collectors. The mass of one foil was approximately 36 mg for Al, 80 mg for Cu, and 250 mg for Au. For the Al and Cu studies, hydrochloric acid (Trace Metal grade, 36–38%, Fisher), nitric acid (metals basis, 65–70%, Alfa Aesar), 18.2 MΩ-cm water (Barnstead GenPure Pro MilliQ water system), n-dodecane (Alfa Aesar, >99%), Tri-n-octylphosphine oxide (ReagentPlus 99%, Aldrich) were all used without further purification. For the Au studies, the hydrochloric acid and water used for dilutions, were Aristar Ultra grade. Commercial resins utilized in this work were Dowex 1x8 (100-200 mesh, Cl form), DGA resin-normal (50-100 μm, Eichrom) and pre-packed Pb resin cartridges (2 mL, 50-100 μm, Eichrom).

2.2. *Beamtime at NSCL*

The ⁸⁸Zr³⁹⁺ secondary beam was generated by fragmentation of a stable 140-MeV/nucleon ⁹²Mo primary beam on a 446-mg/cm² Be target. Using the A1900 fragment separator, ⁸⁸Zr was selected with a 2% momentum acceptance and delivered to the target endstation (Figure 1). The ⁸⁸Zr beam was implanted in the collector attached to the target endstation, which contained the foils of interest. The circular foils were mounted as stacks and clamped with an aluminum ring to an aluminum KF40 flange blank, making up a collector. The collector foils were Al, Cu, W, and Au, with each collector only containing foils of one of these metals. Ten to twenty foils comprised a single collector stack for each material, determined by modeling the stopping ranges using LISE++ and SRIM; tantalum backing foils, to ensure the

¹ Experiments involving W foils will be presented in a separate manuscript.

^{88}Zr beam was completely stopped in the collector stacks, and degraders (for Al, Cu, Au) were also used (Table 1). Tantalum degraders and backing foils were included to ensure the beam was fully stopped in the collector foil stacks. Each collector was irradiated for approximately 8 hours with the ^{88}Zr beam. To monitor the ^{88}Zr beam current on target over the course of the experiment, an intercepting Faraday cup located immediately upstream of the endstation was periodically inserted to read the beam current.

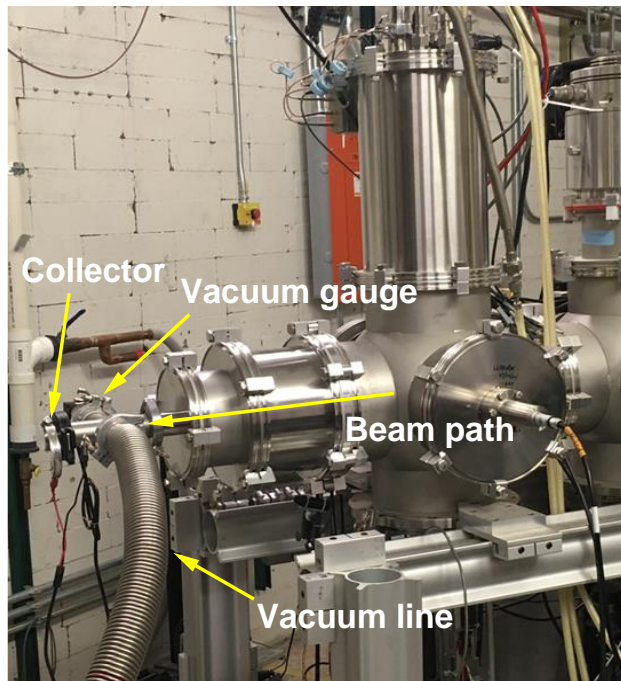


Figure 1: Photograph of the target endstation at the NSCL. Each collector containing the foil stacks for a particular element was secured to the beamline, as shown, and held under vacuum during irradiation with the secondary ^{88}Zr beam.

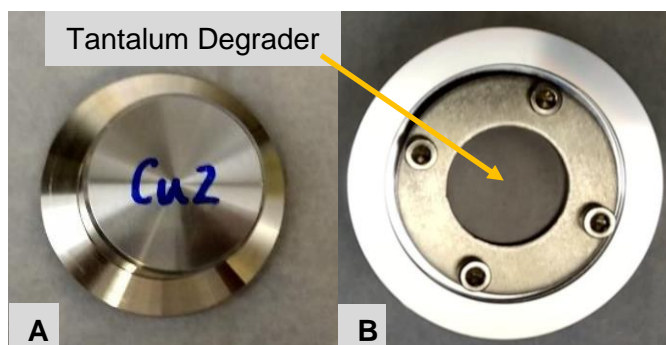


Figure 2: (A) Back of the Cu collector. (B) Front side of the Cu collector with part of the Ta degrader showing, beneath which lies the stack of Cu foils all secured with an aluminum ring and screws. This was mounted onto the end of the beamline as depicted in Figure 1.

Table 1: Contents of each collector, where Ta degraders (0.127 mm thick each) were placed upstream of the target stack and Ta backings were placed downstream behind the foils.

Material	Aluminum (Al)	Copper (Cu)	Tungsten (W)	Gold (Au)
Number of foils in collector	20	16	10	16
Thickness of each foil (mm)	0.025	0.025	0.05	0.025
Purity (%)	99.45	99.8	99.95	99.95
Number of Tantalum Degraders	3	2	None	1
Number of Tantalum Backings	1	1	1	1

Collector stacks were counted on a PHDS Fulcrum portable high purity germanium (HPGe) γ -ray detector outside of the vault within 10 minutes of end of bombardment (EOB) to identify short-lived species. A typical γ -ray spectrum collected immediately after EOB is shown in Figure 6. In addition to ^{88}Zr , other detected radionuclides include: ^{86}Zr ($t_{1/2} = 16.5$ hours), ^{89}Zr ($t_{1/2} = 78.41$ hours), ^{86}Y ($t_{1/2} = 14.74$ hours), ^{87}Y ($t_{1/2} = 79.8$ hours), $^{87\text{m}}\text{Y}$ ($t_{1/2} = 13.37$ hours), and ^{90}Nb ($t_{1/2} = 14.6$ hours). (Basu and Mccutchan, 2020; Johnson and Kulp, 2015; Negret and Singh, 2015; Singh, 2013) Within 24 hours of EOB, the collector stacks were transported from the NSCL to the radiochemistry laboratory in the MSU Department of Chemistry for further analysis. Each collector was disassembled, and the individual foils were counted on a shielded HPGe detector to determine the identity and distribution of beam products in the stacks. After the initial analysis, the W collector foils remained at MSU while the Cu and Al collector foils were shipped to Hunter College and the Au collector foils were shipped to Lawrence Livermore National Laboratory (LLNL) for subsequent separation chemistry for the extraction of ^{88}Zr and ^{88}Y .

2.3. Autoradiography of Gold Foils at LLNL

The gold foils were used as a representative set to examine the beam spot shape and distribution using autoradiography. The three most active foils (Au #11, 12 and 13), with respect

to ^{88}Zr , were exposed to an SR BAS phosphor storage plate through a plastic bag for 8 hours. The phosphor plates were then scanned with a Typhoon FLA 7000 and the generated autoradiographs were analyzed by ImageJ software.

2.4. Separation of ^{88}Zr and ^{88}Y from Aluminum Foils

Harvesting from the Al foils was performed 1 month after EOB; therefore, the only remaining detectable radionuclides were ^{88}Zr ($t_{1/2} = 83.4$ d), its daughter ^{88}Y ($t_{1/2} = 106.626$ days), and ^{85}Sr ($t_{1/2} = 64.849$ days). (McCutchan and Sonzogni, 2014, p. 88; Singh and Chen, 2014, p. 85) Foils were counted on an Ortec GEM60P4 HPGe detector. Those containing deposited ^{88}Zr were cut in halves or quarters for subsequent chemical processing.

Each Al foil fragment was dissolved in 500 μL of concentrated HCl with 10 μL of concentrated HNO_3 in a hot water bath with stirring for 1 hour. The Al solution was evaporated to a wet residue and reconstituted in concentrated HCl several times to remove residual nitric acid and keep ^{88}Zr in solution as a free anionic complex. During this step, a portion of the Al precipitates as insoluble hydrated aluminum chloride. Approximately 500 μL of supernatant was removed and allowed to cool, counted on a 1.1 x 2 cm NaI well detector (Alpha Spectra Inc.), then loaded onto a prepared strong-base anion-exchange resin (Dowex 1x8 100-200 mesh Cl⁻ form, 2 mL column volume, 4 cm x 0.8 cm). The column was prepared by slurry loading resin preconditioned with 1 M HCl, then washed with >10 column volumes (CVs) of concentrated HCl with gravity flow. The loading solution vial was rinsed twice with an additional 500 μL of concentrated HCl and added to the column to ensure all the ^{88}Zr was loaded. The column was washed with concentrated HCl for a total of 22.5 mL (>11 CVs) to elute both cationic Al^{3+} and $^{88}\text{Y}^{3+}$. A total of 25 mL (>12 CVs) of hot 6 M HCl was used to elute the ^{88}Zr . Each fraction was counted on the NaI detector in the same geometry as the load solution to determine final recovery of ^{88}Zr . An identical, non-radioactive surrogate experiment without ^{88}Zr or ^{88}Y was performed to determine the elution profile of Al. Al was quantified using inductively coupled plasma optical emission spectroscopy (ICP-OES) using a Shimadzu ICPE-9000 Multitype ICP Emission Spectrometer at 258 nm wavelength for each collected fraction.

To isolate the ^{88}Y , fractions containing ^{88}Y that co-eluted with Al in the initial anion-exchange column were loaded onto normal DGA resin, which has a N,N,N',N'-tetra-n-octyldiglycolamide functional group that strongly binds to trivalent rare earths and high field strength elements. (Ansari et al., 2012; Horwitz et al., 2005; Pourmand and Dauphas, 2010) DGA resin has a high affinity for Y^{3+} in a wide range of hydrochloric and nitric acid concentrations, while Al exhibits low sorption to the resin in all acid concentrations. (Horwitz et al., 2005) DGA resin was pre-wetted with 1 M HCl for 24 hours and slurry loaded into a column yielding a 0.5 mL CV (0.4 cm x 1 cm), then pre-conditioned with 10 CVs of concentrated HCl. Fractions containing ^{88}Y and Al in concentrated HCl from the previous ^{88}Zr separation (1.5 mL each) were counted on a NaI detector, then loaded directly onto the prepared column under gravity flow. The column was washed with concentrated HCl, collecting the 12 mL of load and wash eluate together. The ^{88}Y was eluted in 9 mL of 1 M HCl followed by 4 mL of water. The full separation scheme for ^{88}Zr and ^{88}Y is shown in Figure 3 below. Decontamination factors (DF) of the target nuclide (^{88}Zr and ^{88}Y) from the Al, Cu and Au foils were calculated using Eq. 1:

$$\text{DF} = \frac{\left(\frac{\text{mol}_{^{88}\text{Zr}}}{\text{mol}_{\text{M}}}\right)_{\text{Final}}}{\left(\frac{\text{mol}_{^{88}\text{Zr}}}{\text{mol}_{\text{M}}}\right)_{\text{Initial}}}$$

Where 'M' indicates the metal (Al or Cu). The limit of quantification of the ICP-OES for Al and Cu was 10 ppb, and thus used as a minimum value for determining mol_M of Al and Cu for samples with a concentration below this value. For the Au separations, ^{88}Y was recovered only from decay of purified ^{88}Zr , therefore decontamination factors of ^{88}Y from Au were not calculated.

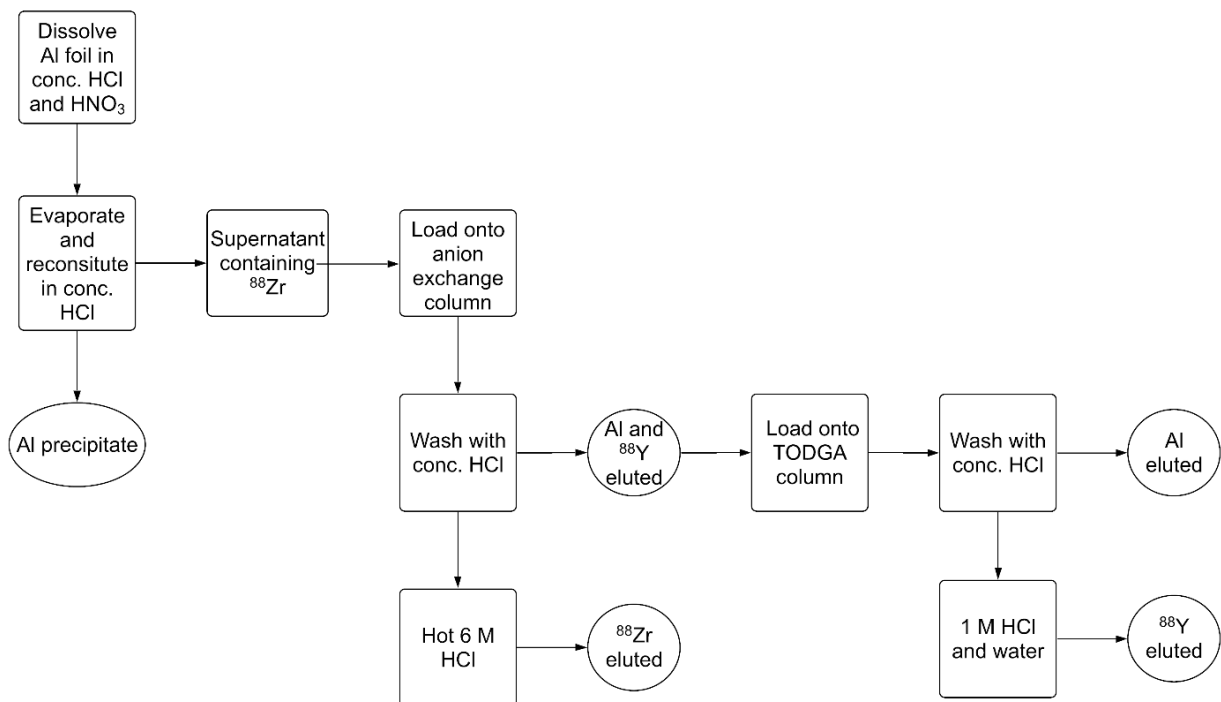


Figure 3: Schematic of the complete separation of ^{88}Zr and ^{88}Y from bulk Al foil.

2.5. Separation of ^{88}Zr and ^{88}Y from Copper

Cu foils were cut in half, dissolving each half in 500 μL of prepared 12 M HNO_3 . The dissolved Cu solution was counted on a NaI detector prior to the separation procedure. 2 mL of 0.01 M trioctylphosphine oxide (TOPO) in n-dodecane was pre-equilibrated with 2 mL of 12 M HNO_3 by mixing each together for 3 minutes, then allowing to settle for 30 minutes. The solution was centrifuged for 2 minutes, then 500 μL of the organic layer was removed and added to the dissolved Cu solution (1:1 volume ratio) for selective extraction of the ^{88}Zr into the organic layer. The two phases were mixed with a vortex mixer for 3 minutes, followed by 3 minutes of centrifugation. The phases were separated with a pipette and the organic layer counted on a NaI detector. The organic layer was washed 3 times with 12 M HNO_3 by adding the organic layer to 500 μL of 12 M HNO_3 , vortex mixing for 3 minutes, and centrifuging for 2 minutes for each wash. By this method, the ^{88}Y and the Cu remained in the 12 M HNO_3 aqueous phase while a majority of the ^{88}Zr was extracted into the organic layer. This process constituted one pass, which was repeated once more with another 500 μL of 0.01 M TOPO in n-dodecane. The organic phases from passes 1 and 2 containing ^{88}Zr were combined and the ^{88}Zr back-extracted by vortex mixing with an equal volume of 1 M HCl for 3 minutes, separating by centrifugation for 2 minutes, and repeating 3 times. The full scheme is shown in Figure 4.

Following ^{88}Zr extraction, ^{88}Y and Cu remained in the initial 12 M HNO_3 aqueous phase (500 μL). To separate the ^{88}Y from the Cu, the mixture was loaded on a DGA resin column, prepared in the same manner as previously described for Al, but here pre-conditioned with 10 CVs of 12 M HNO_3 . After loading, the column was washed with 10 CVs 12 M HNO_3 , and eluted sequentially with 20 CVs 0.1 M HNO_3 , 20 CVs 1 M HCl , and 20 CVs water.

Identical non-radioactive surrogate experiments without ^{88}Zr or ^{88}Y were performed for both the solvent extraction and column separations to determine the Cu concentration of the solutions at each step in the procedure. Cu was quantified using ICP-OES at 225 nm wavelength for each sample.

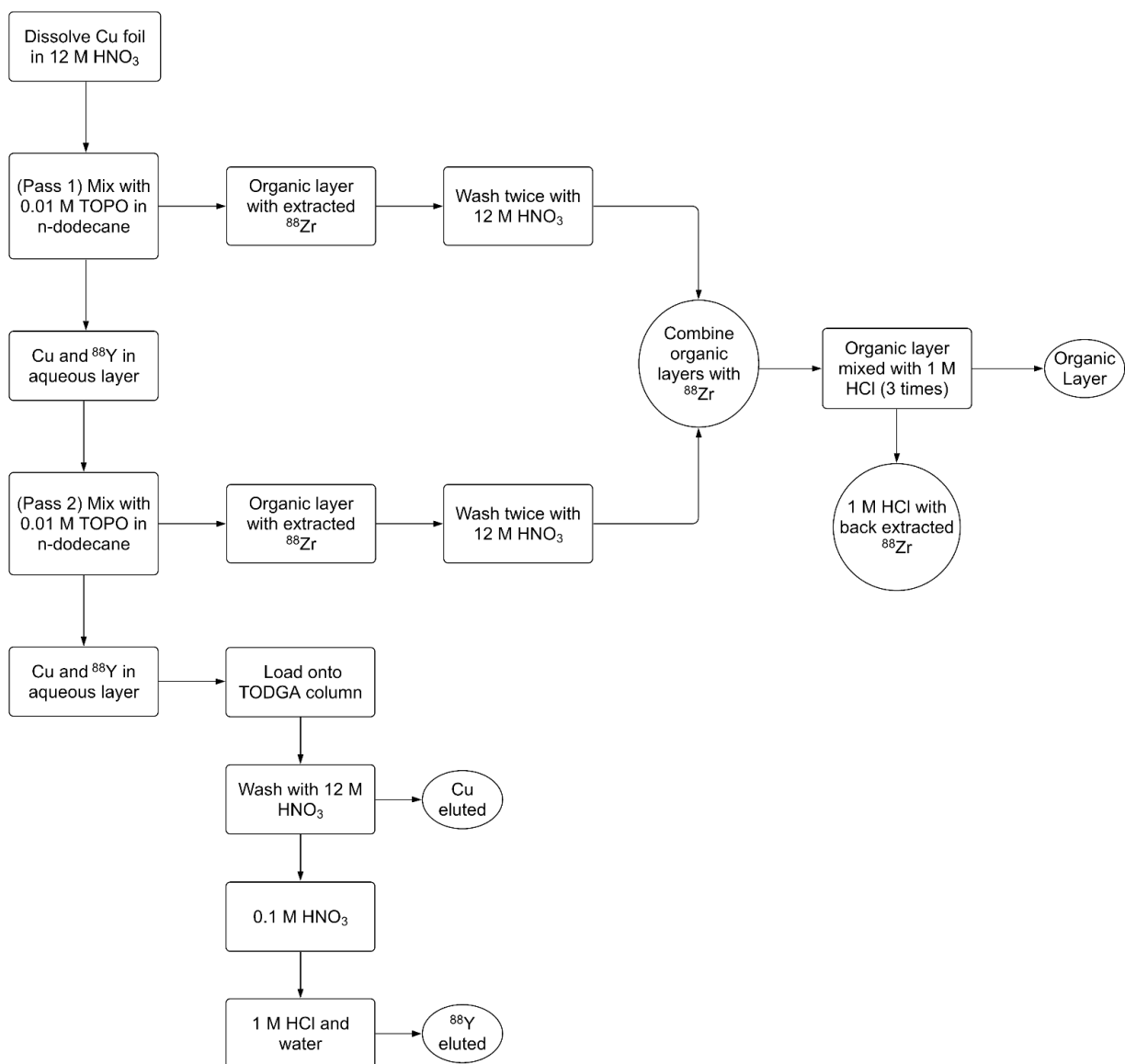


Figure 4: Schematic of the complete separation for the extraction of ^{88}Zr and ^{88}Y from bulk Cu foil.

2.6. Separation of ^{88}Zr and ^{88}Y from Gold

Each Au foil was counted by standard coaxial HPGe gamma-ray detectors at Lawrence Livermore National Laboratory's Nuclear Counting Facility (NCF) and analyzed with LLNL's GAMANAL software to determine the absolute activity of ^{88}Zr present in each foil. A representative measure of the beam spot on the foils from the ^{88}Zr beam was obtained through digital autoradiography using SR-BAS phosphor storage plates and a GE Typhoon FLA7000 scanner. The chemistry to separate ^{88}Zr from Au was started 4 months after EOB, at which point the radionuclides present were ^{88}Zr , ^{88}Y , and ^{85}Sr . The three most active foils: Foil #11 (245 mg), #12 (255 mg) and #13 (251 mg), were each dissolved in 4 mL of aqua regia, then evaporated to dryness and reconstituted in 6 mL of 4 M HCl. Each dissolved foil solution was split into three 2 mL load fractions, for a total of 9 load fractions. Nine stacks of three columns, each comprised of two 2 mL pre-packed Pb resin cartridges stacked on an Eichrom prefilter cartridge (for removal of organics), were prepared on a vacuum box and conditioned with 10 mL (2.5 CVs) of 4 M HCl at a flow rate of 2 mL/min. Each load fraction was added to its respective column stack in 4 M HCl, in which ^{88}Zr and ^{88}Y pass through the column and were fully eluted with 15 mL (3.75 CVs) of 4 M HCl. The Au was removed from the column with 10 mL of concentrated HNO_3 , (Despotopulos and Kmak, 2021) but was not quantified. For each foil, the ^{88}Zr fractions from the three columns were combined and evaporated to dryness. These were reconstituted in 10 mL concentrated HCl and counted at the NCF for ^{88}Zr yields. A 1 mL aliquot of this solution was then taken for inductively coupled plasma mass spectrometry (ICP-MS) analysis using a Thermo Scientific iCAP quadrupole ICP-MS to determine the amount of Au remaining in the solution.

Following the removal of Au from the ^{88}Zr and ^{88}Y and subsequent analysis, separation of ^{88}Zr from ^{88}Y was done 10 months after EOB. The remaining 9 mL of ^{88}Zr solution from the most active foils, #11 and #12, was evaporated to dryness and reconstituted in 1 mL of 13 M HCl (prepared by bubbling HCl gas into concentrated HCl). This solution was counted with a coaxial HPGe detector to determine the initial activities of ^{88}Zr and ^{88}Y present in the solutions. Two, 1 mL column volume (0.7 cm x 3 cm) anion-exchange columns were prepared and conditioned with 5 mL (5 CVs) of 13 M HCl. Each foil solution was loaded onto a separate column and ^{88}Y was eluted with four 1 mL fractions (4 CVs) of 13 M HCl. The ^{88}Zr was then eluted with six 1 mL fractions (6 CVs) of 4 M HCl, all with gravity flow. Each fraction was counted on the same HPGe detector in the same geometry as the load solution and the spectra were analyzed with ORTEC's Maestro software. Figure 5 shows the complete separation scheme for ^{88}Zr and ^{88}Y from Au.

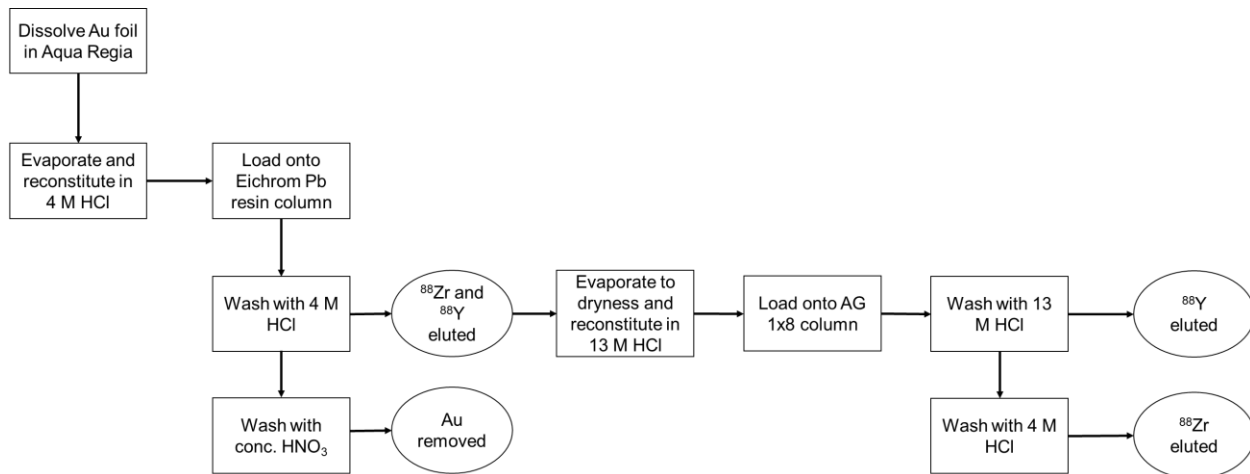


Figure 5: Schematic of the complete separation scheme for the extraction of ^{88}Zr and ^{88}Y from bulk Au foil.

3. Results/Discussion

3.1. *Post-Irradiation Analysis*

Once chemistry on the foils began about one month after EOB, most of the beam products other than ^{88}Zr and its decay product ^{88}Y had decayed to below detectable levels. The exception was ^{85}Sr , which was detected several months post-irradiation in all three collector materials, however detailed quantification was only possible for the Au foil stack. The beam product deposition agreed with the stopping range calculations with the ^{88}Zr collecting in foils #6-11 for the Al stack, #12-15 for the Cu stack, and #1-13 foils for the Au stack (Figures 7, 8, and 9 for Al, Cu, and Au, respectively). The number of atoms of ^{88}Zr deposited in the collectors exceeded other products by at least one order of magnitude. The predicted ion transmission rate into a collector for ^{88}Zr from LISE++ software was 1.56×10^6 particles per second (pps).

The decay corrected total activity of ^{88}Zr deposited into the collector stacks are shown in Table 2. The difference in deposited activity in the collectors is due to the variations in integrated particle rates from collector to collector. Au had the highest average particle rate (in atoms of ^{88}Zr per second) at $(2.39 \pm 0.08) \times 10^7$ compared to Al and Cu $(2.12 \pm 0.13) \times 10^7$ and $(1.82 \pm 0.09) \times 10^7$, respectively, as determined by γ -ray spectroscopy analysis decay corrected to end of bombardment. While no ^{88}Zr was detected in the KF40 flange, Ta degrader foils, Ta backing foils, or metal screws, $(5.6 \pm 2.2) \%$, $(4.1 \pm 2.3) \%$ and $(6.8 \pm 3.4) \%$ of the total ^{88}Zr activity was deposited onto the Al ring clamp for the Al, Cu and Au collectors, respectively.

Table 2: Experimentally determined total activity, number of atoms, and particle rates of ^{88}Zr for each collector stack.

Collector	Activity of ^{88}Zr at EOB (Bq)	Number of ^{88}Zr atoms at EOB	Integrated beam on target time (hours)	Average particle rate of ^{88}Zr (pps)
Al	$(5.72 \pm 0.36) \times 10^4$	$(5.94 \pm 0.37) \times 10^{11}$	7.78	$(2.12 \pm 0.13) \times 10^7$
Cu	$(3.87 \pm 0.20) \times 10^4$	$(4.02 \pm 0.21) \times 10^{11}$	6.15	$(1.82 \pm 0.09) \times 10^7$
Au	$(6.41 \pm 0.22) \times 10^4$	$(6.66 \pm 0.23) \times 10^{11}$	7.75	$(2.39 \pm 0.08) \times 10^7$

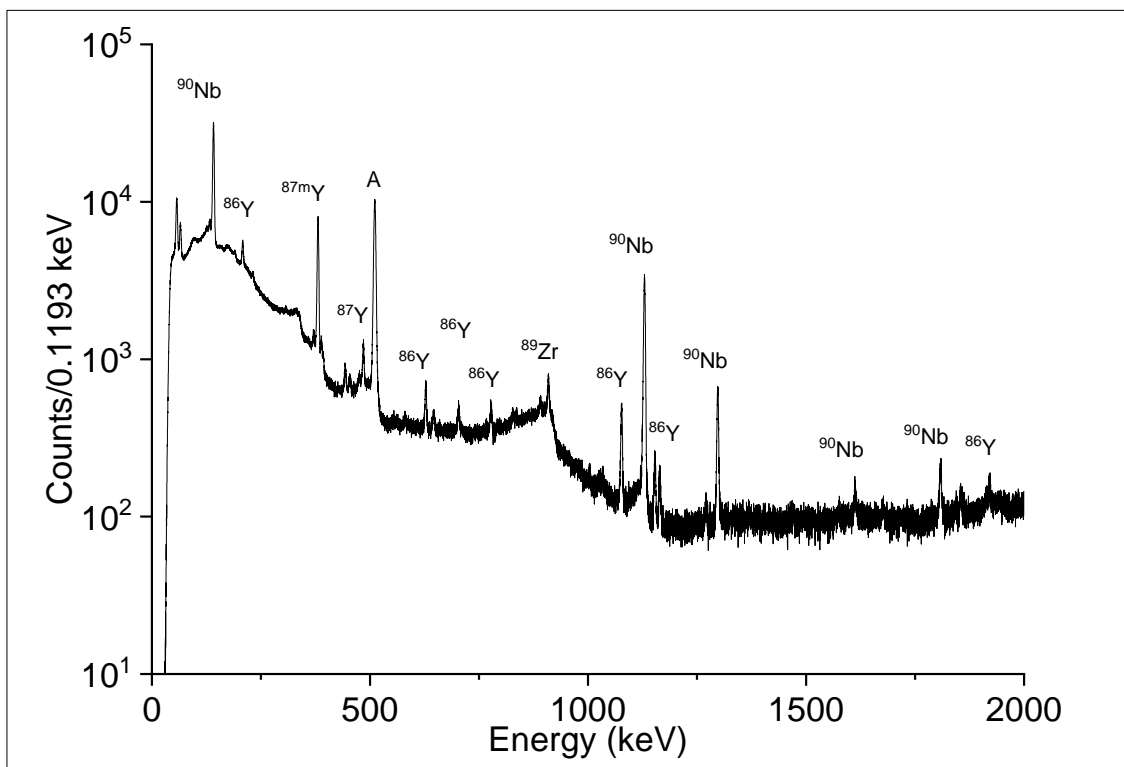


Figure 6: HPGe γ -ray spectrum of the Cu collector following removal from the target endstation. The spectrum was collected within 30 minutes of EOB and is not decay corrected. Beam products co-deposited with the ^{88}Zr shown in the spectrum include ^{86}Zr , ^{89}Zr , ^{86}Y , ^{87}Y , $^{87\text{m}}\text{Y}$, and ^{90}Nb . The peak labeled "A" is the 511 keV annihilation peak.

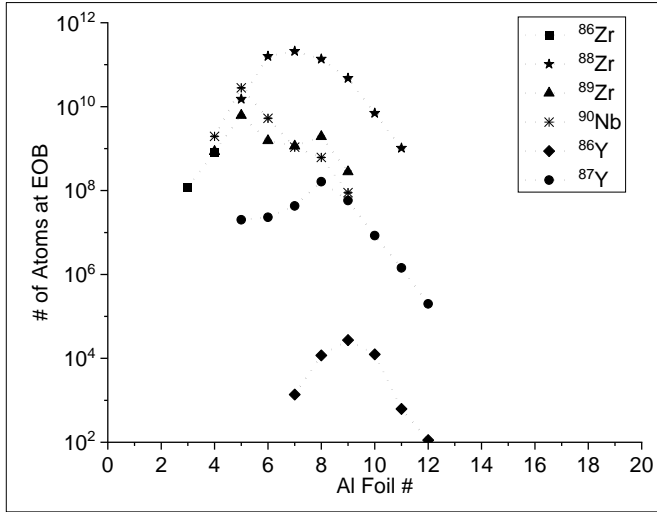


Figure 7: Distribution of beam products in the Al collector in number of atoms, decay corrected to EOB. Counting of the individual Al foils began within 6 hours from EOB. The x-axis represents each foil in the stack, with foil #1 the most upstream and first to be hit by the beam, and foil #20 the most downstream. Note that the Ta degraders and backing foils have been left out of this figure as no activity was detected on these components. No activity was detected on foils #1, 2, or 13-20. ^{88}Zr was detected in foils #5-11, denoted by stars.

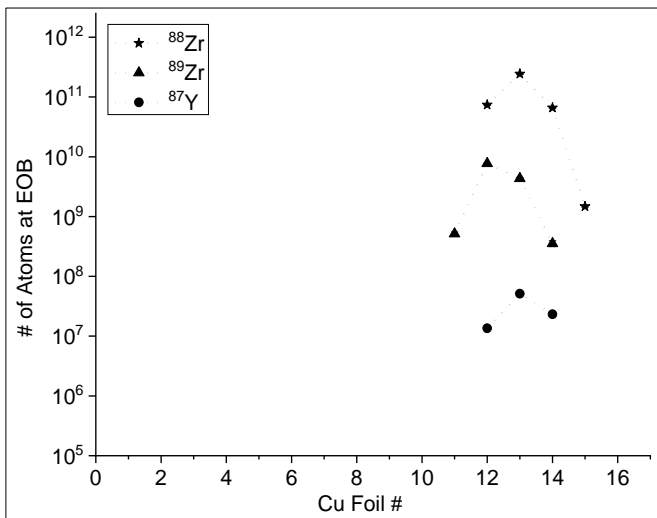


Figure 8: Distribution of beam products in the Cu collector in number of atoms, decay corrected to EOB. Foils were counted 9 days after EOB, so many of the short-lived species had decayed away before they could be detected. The x-axis represents each foil in the stack, with foil #1 the most upstream and first to be hit by the beam, and #16 the most downstream. Note that the Ta degraders and backing foils have been left out of this figure as no activity was detected on these components. At 9 days post EOB, no activity was detected in foils #1-10 or 16. ^{88}Zr was detected in foils #12-15, denoted by stars. Cu and Au foils, however, were not analyzed the same day as EOB, resulting in fewer short-lived beam products detected compared to the Al foils.

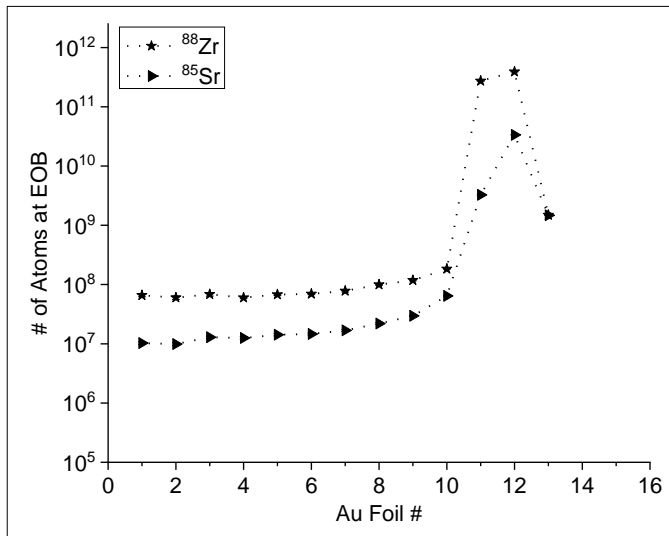


Figure 9: Distribution of beam products in the Au collector in atoms, decay corrected to EOB. Foils were counted 3 months after EOB, so the short-lived species had decayed to below detectable levels. The x-axis represents each foil in the stack, with foil #1 the most upstream and the first to be hit by the beam, and #16 the most downstream. Note that the Ta degraders and backing foils have been left out of this figure as no ⁸⁸Zr was detected in these components. No activity was detected on foils #14-16.

3.2. Autoradiography

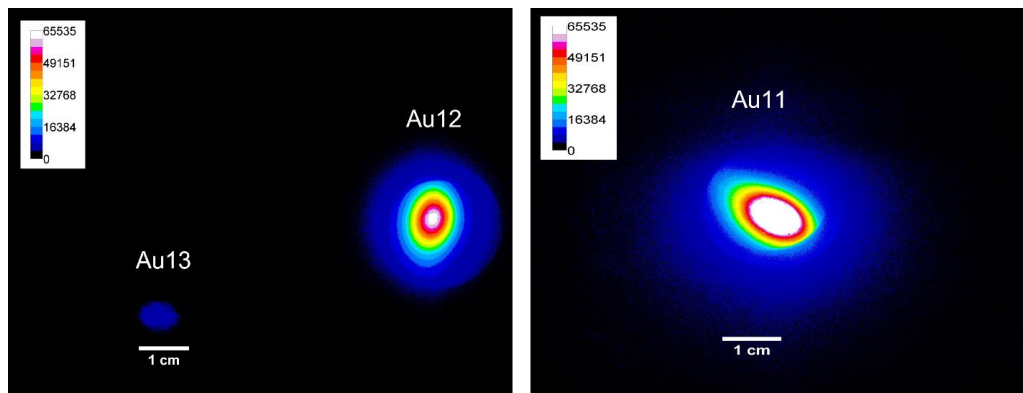


Figure 10: Autoradiographs of Au foils #11, #12 and #13. The false color scale corresponds to the amount of energy deposited into each pixel on the image plate, with a higher number indicating more radiation emanating from that point. The autoradiography analysis of the three most active Au foils indicate that the beam spot was centrally located in the Au foil. For the most active foils, #11 and #12, the activated portion of the image plate was an oval approximately 1.5 cm long and 0.75 cm wide, indicating that the beam spot was an oval slightly smaller in size. Autoradiographs were not recorded for Al or Cu foils.

3.3. Harvesting of ^{88}Zr and ^{88}Y from Aluminum foils

In concentrated HCl, Zr is predominantly in the form $[\text{ZrCl}_6]^{2-}$, which is strongly adsorbed on the anion-exchange resin. In 6 M HCl, neutral complexes such as ZrCl_4 are the dominant form and weakly adhere to the resin, allowing for elution of ^{88}Zr from the column in this matrix. (Kraus and Nelson, 8/7; Wang and Lee, 2016) ICP-OES analysis of Al in the non-radioactive surrogate experiments showed (56 ± 6.7) % of the total Al mass was removed via the initial precipitation, with the remainder being separated from the ^{88}Zr in the concentrated HCl elution from the anion-exchange column. prior to the anion-exchange step. The total recovery of ^{88}Zr was (86.6 ± 5.4) % over five trials, with an average decontamination factor of 2.2×10^5 (Table 3). While no Al was detected in the final ^{88}Zr fractions, the limit of quantification of 10 ppb for Al in the ICP-OES for each fraction set the upper limit of Al concentration used for decontamination factor calculations. The unrecovered ^{88}Zr remained with the Al precipitate ($\sim 2\%$) or was retained on the column ($\sim 11\%$).

After separation with DGA, the average ^{88}Y recovery from Al over 3 trials was (93.1 ± 4.5) % with a decontamination factor of 2.8×10^5 . Unrecovered ^{88}Y was retained on the DGA column with no other losses. Chromatograms of Al, ^{88}Y , and ^{88}Zr from anion-exchange and DGA separations are shown in Figures 11 and 12, respectively. A typical γ -ray spectrum of one of these fractions is shown in Figure S1, where the only nuclide other than ^{88}Zr was the in-grown daughter ^{88}Y , present from decay during the time between column elution and counting the fractions. The non-radioactive surrogate experiment showed (102 ± 5.7) % elution of Al from the DGA column in the concentrated HCl column fractions. No Al was detected in the fractions where 1 M HCl and water was used as eluent.

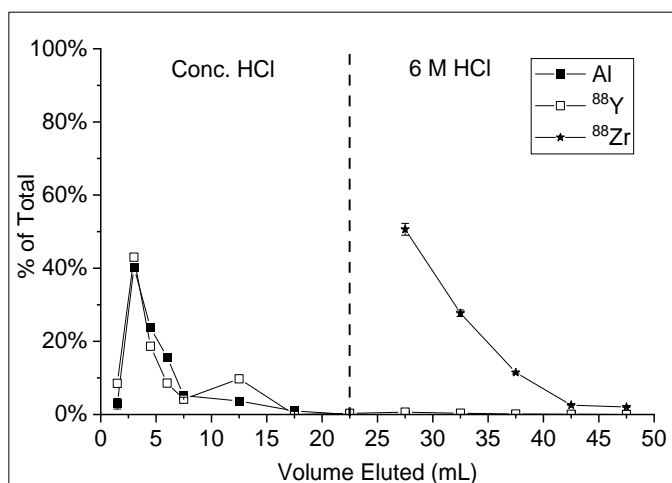


Figure 11: Sample elution curves from anion-exchange resin separation of ^{88}Zr from bulk Al in HCl. Y-axis values are reported as percent of total Al content by mass or percent of the total activity of ^{88}Zr and ^{88}Y . The Al data were collected in a separate non-radioactive separation run under identical conditions to the radioactive samples to allow for ICP-OES analysis. Lines are only to guide the eye.

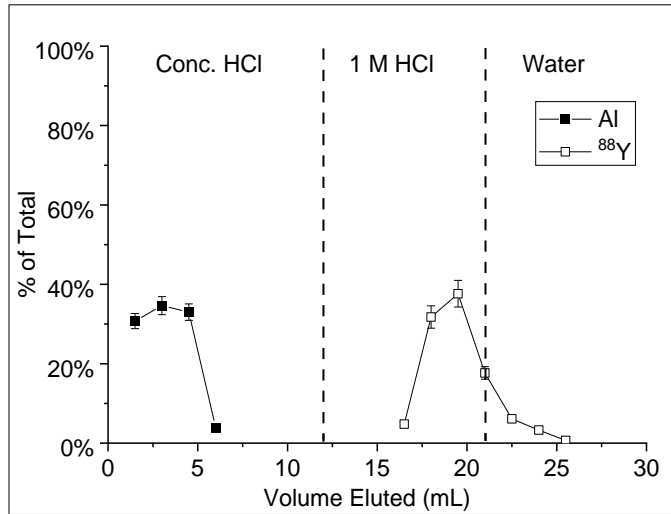


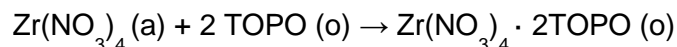
Figure 12: Elution curves from DGA resin separation of ⁸⁸Y from bulk Al in HCl. Y-axis values are reported as percent of total Al content by mass or percent of the total activity of ⁸⁸Y. The Al data were collected in a separate, non-radioactive separation under identical conditions to the radioactive samples to allow for ICP-OES analysis. Lines are only to guide the eye.

Table 3: Total recovery yields for each separation of ⁸⁸Zr from bulk Al foils.

Trial #	Mass of Al (mg)	Total ⁸⁸ Zr activity (Bq)	⁸⁸ Zr recovered (%)	Decontamination Factor
Al #1	10.9	55 ± 3	82.5 ± 5.5	1.8 x 10 ⁵
Al #2	9.7	223 ± 14	91.6 ± 6.3	1.8 x 10 ⁵
Al #3	9.6	1060 ± 59	89.4 ± 5.6	1.7 x 10 ⁵
Al #4	16.0	2420 ± 110	81.1 ± 4.5	2.6 x 10 ⁵
Al #5	17.5	1640 ± 81	88.6 ± 5.0	3.1 x 10 ⁵

3.4. Harvesting of ^{88}Zr and ^{88}Y from Copper foils

From acidic solutions, Zr can be complexed by both acidic or neutral organophosphorus extractants. (Banda et al., 2013; Saisho, 1962; Wang et al., 2013) This property has been exploited in many applications for selective solvent extraction of Zr from mixtures, such as in the separation of Zr from Hf. (Wang and Lee, 2016) The neutral trioctylphosphine oxide (TOPO) ligand has been used to extract Zr from acidic solutions of hydrochloric or nitric acid into the organic phase. (Banda et al., 2013; Biswas and Basu, 1999; Saisho, 1962; White and Ross, 1958) The extraction typically follows the following solvating scheme:



Where (a) is the aqueous phase and (o) is the organic phase containing the TOPO extractant. (Wang and Lee, 2016; White and Ross, 1958)

The strong extraction of Zr^{4+} with TOPO in n-dodecane from acidic matrices combined with poor extraction of divalent and trivalent metals allowed for separation of Zr from both Cu and its decay product ^{88}Y . ^{88}Zr was quantitatively extracted from the 12 M HNO_3 to the organic phase with 0.01 M TOPO solution after two passes. 12 M HNO_3 was determined to be the best nitrate medium that struck a balance between extraction efficiency and back-extraction efficacy; higher concentrations of HNO_3 improved extraction effectiveness of ^{88}Zr but decreased back-extraction in 1 M HCl. Lower concentrations of HNO_3 decreased extraction efficiency and increased likelihood of ^{88}Zr hydrolysis. ICP-OES analysis showed <0.5% of the original Cu mass present in the first HNO_3 wash solution, followed by <0.05% in the second of the three HNO_3 washing solutions, likely due to co-extraction from the first pass of TOPO. No Cu was detected in the third HNO_3 wash or any of the 1 M HCl solutions used for back extraction. The limit of quantification of 10 ppb for the ICP-OES for Cu in each sample set the upper limit of Cu concentration used for decontamination factor calculations. The average yield of ^{88}Zr recovered from Cu was $(88.4 \pm 5.4) \%$ with a decontamination factor of 3.3×10^5 (Table 4). The unrecovered ^{88}Zr remained in the nitric acid wash solutions as well as in the organic phase after back extraction.

After subsequent separation with DGA, the average ^{88}Y recovery from Cu over 4 trials was $(96.2 \pm 4.1) \%$ with a decontamination factor from Cu of 3.7×10^5 . Unrecovered ^{88}Y remained adhered to the walls of vials used to dissolve the Cu foils. The elution curves for Cu and ^{88}Y are shown in Figure 13. Similar to the separation of Al and ^{88}Y , DGA resin has poor uptake of Cu complexes in nitric acid, allowing for selective chelation of ^{88}Y , which is strongly retained in high concentrations of HNO_3 .

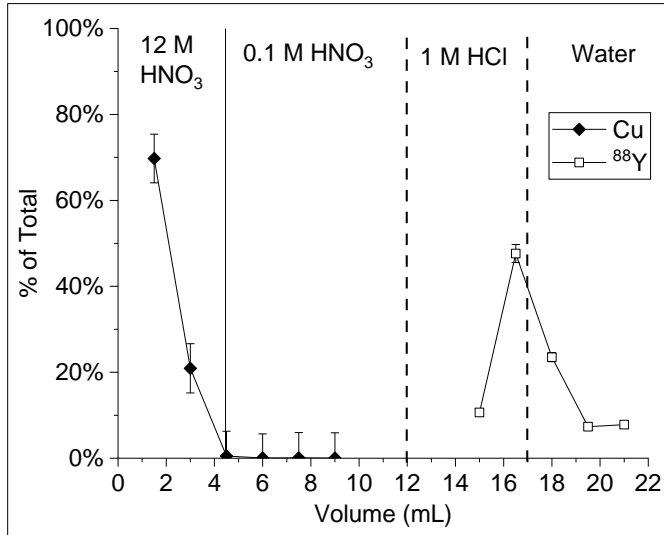


Figure 13: Elution curves from DGA resin for separation of ⁸⁸Y from bulk Cu in HNO₃ and HCl. Y-axis values are reported as percent of total Cu content by mass or percent of the total activity of ⁸⁸Y. The Cu data were collected in a separate non-radioactive separation under identical conditions to the radioactive samples to allow for ICP-OES analysis. Lines are only to guide the eye.

Table 4: Total recovery yields for each separation of ⁸⁸Zr from bulk Cu foils.

Trial #	Mass of Cu (mg)	Total ⁸⁸ Zr activity (Bq)	⁸⁸ Zr recovered (%)	Decontamination Factor
Cu #1	43.3	754 ± 41	90.2 ± 5.4	3.3 × 10 ⁵
Cu #2	46.0	2260 ± 112	89.3 ± 4.9	3.5 × 10 ⁵
Cu #3	43.7	77 ± 4	89.6 ± 5.7	3.3 × 10 ⁵
Cu #4	42.6	58 ± 3	84.5 ± 5.6	3.1 × 10 ⁵

3.5. Harvesting of ^{88}Zr and ^{88}Y from Gold

Following the dissolution of Au in aqua regia, evaporation, and reconstitution in 4 M HCl, Au is present as AuCl_4^- . The crown ether extractant on the Pb resin strongly binds the Au anion through an association complex with a positively charged crown ether-hydronium ion complex. (Camagong and Honjo, 2001; Despotopulos and Kmak, 2021) Table 5 shows the total recovery yields for each ^{88}Zr separation from bulk Au foils. The average yield of ^{88}Zr recovered from Au was $(98.8 \pm 13.5)\%$ with a decontamination factor of 4.3×10^6 . Decontamination factors for ^{88}Zr from Au are higher than those from the Al and Cu due to lower limit of detection of the ICP-MS (<1 ppb) used in the Au work compared to that of the ICP-OES used for the Al and Cu studies.

Table 5: Total recovery yields for each separation of ^{88}Zr from bulk Au foils.

Foil #	Mass of Au (mg)	Total ^{88}Zr activity (Bq)	^{88}Zr recovered (%)	Decontamination Factor
Au #11	245	$(2.65 \pm 0.11) \times 10^7$	98.1 ± 4.2	4.1×10^6
Au #12	255	$(3.80 \pm 0.16) \times 10^7$	103.5 ± 4.3	5.6×10^6
Au #13	251	$(1.44 \pm 0.10) \times 10^5$	96.2 ± 7.2	4.0×10^7

As can be seen from Table 5, the initial debulking of Au resulted in greater than 95% recovery of ^{88}Zr , with each 2 mL pre-packed Eichrom Pb resin cartridge having an approximate Au capacity of 50 mg. (Despotopulos and Kmak, 2021) The latter $^{88}\text{Zr}/^{88}\text{Y}$ anion exchange separation followed the same principles previously described for Al with the elution of a neutral ZrCl_4 in 4 M HCl. The recovery of both ^{88}Zr and ^{88}Y from the anion exchange separations was consistent with 100%, with large uncertainties due to poor counting statistics (Table 6). No ^{88}Zr or ^{88}Y was measured on the column or in the empty load tube.

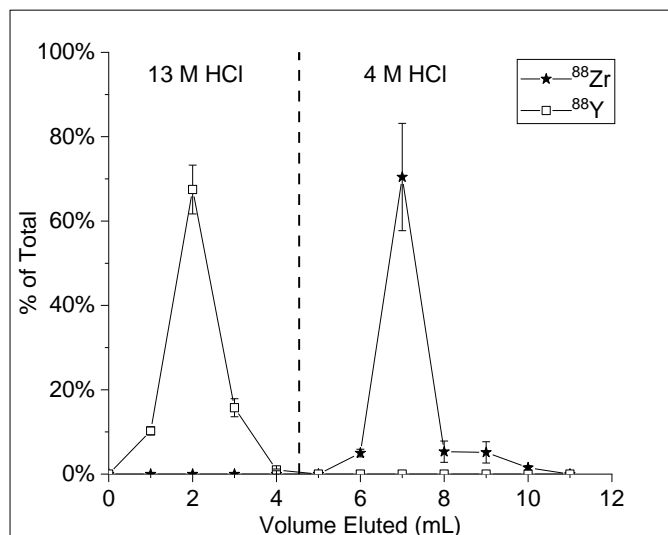


Figure 14: Separation of ^{88}Y from ^{88}Zr using AG 1x8 (100-200 mesh) from Au foil #11. Similar results were reproduced for Au foil #12. Lines are to guide the eye.

Table 6: Recovery yields for ^{88}Zr and ^{88}Y separation with AG 1x8.

Foil #	^{88}Zr Recovery (%)	^{88}Y Recovery (%)
Au #11	87.4 ± 13.3	94.4 ± 6.2
Au #12	110.2 ± 13.6	103.1 ± 6.6

4. **Conclusion**

Total yields of ^{88}Zr were (86.6 ± 5.4) % from Al, (88.4 ± 5.4) % from Cu, and (98.8 ± 13.5) % from Au for an average recovery of (91.3 ± 8.9) % and average decontamination factor of 4.3×10^6 . The solid-phase collection in this work showed more than three times increase in ^{88}Zr recovery compared to previous aqueous-phase isotope harvesting efforts. The higher recoveries of ^{88}Zr are attributed to maintaining the extractable Zr^{4+} species in highly acidic conditions once in solution to avoid formation of hydrolysis products. The only detectable radioactive contaminant present at time of separation was the in-grown ^{88}Y daughter, which was also successfully separated from both ^{88}Zr and the bulk collector materials. Yields of ^{88}Y were (93.1 ± 4.5) % from Al, (96.2 ± 4.1) % from Cu, and (95.7 ± 8.0) % from Au for a total average recovery of (95.0 ± 5.8) %. The average decontamination factor of ^{88}Y from Al and Cu was 3.3×10^5 . The average time from dissolution to finished separation of both ^{88}Zr and ^{88}Y from Al, Cu and Au was 6 hours, 4 hours, and 5 hours, respectively. This timeline could be shortened with the use of a peristaltic pump or even future adaptation to a liquid chromatography system, potentially improving the efficiency of the separations without compromising the high recovery yields.

A proof-of-concept experiment for solid-phase isotope harvesting of ^{88}Zr from Al, Cu, W, and Au collectors was demonstrated at the NSCL for application to FRIB. Foil stacks of each material were irradiated with an ^{88}Zr secondary beam, then chemically processed to recover and purify the deposited ^{88}Zr using a combination of anion-exchange chromatography, extraction chromatography and solvent extraction techniques. These separation methodologies developed for ^{88}Zr provide a framework for harvesting Zr isotopes, other group IV elements, or elements with complex aqueous chemistry that may be better suited for solid-phase isotope harvesting. The separations here were aided by the decay of the short-lived species, however, they represent some of the dominant species even at EOB. Future experiments targeting shorter-lived products may require more complex separations schemes to accommodate the presence of more radionuclides, such as Nb isotopes in the case of harvesting neutron-deficient Zr. With FRIB recently commencing operation, expanding the isotope harvesting toolkit will make a wider array of radionuclides available to the nuclear-science community.

Acknowledgements

We thank the staff at the NSCL for providing beam for this experiment, especially considering the challenges associated with the COVID-19 pandemic. Thank you to Lynn Francesconi at Hunter College for use of her laboratory spaces and guidance. Thank you to Eric Norman for use of his HPGe detector for some of this work. Thank you to Sam Groveman from Medgar Evers College of the City University of New York for ICP-OES analyses. Thank you to the NCF staff, Keenan Thomas and Todd Woody, at LLNL for initial gamma counting of the Au foils. We also thank Rachel Lindvall at LLNL for the ICP-MS analysis. This research is supported by the U.S. Department of Energy Isotope Program, managed by the Office of Science for Isotope R&D and Production under contract DE-SC0020161. This work was performed under the

auspices of the U.S. Department of Energy by Lawrence Livermore National Laboratory under Contract DE-AC52-07NA27344. At MSU, this work was supported by the Core R&D Support for Isotope Harvesting at FRIB as part of the DOE-SC-Isotope Program under Contract DE-SC0021220.

References

- Abel, E.P., Avilov, M., Ayres, V., Birnbaum, E., Bollen, G., Bonito, G., Bredeweg, T., Clause, H., Couture, A., DeVore, J., Dietrich, M., Ellison, P., Engle, J., Ferrieri, R., Fitzsimmons, J., Friedman, M., Georgobiani, D., Graves, S., Greene, J., Lapi, S., Loveless, C.S., Mastren, T., Martinez-Gomez, C., McGuinness, S., Mittig, W., Morrissey, D., Peaslee, G., Pellemoine, F., Robertson, J.D., Scielzo, N., Scott, M., Severin, G., Shaughnessy, D., Shusterman, J., Singh, J., Stoyer, M., Sutherlin, L., Visser, A., Wilkinson, J., 2019. Isotope harvesting at FRIB: additional opportunities for scientific discovery. *J. Phys. G: Nucl. Part. Phys.* 46, 100501. <https://doi.org/10.1088/1361-6471/ab26cc>
- Abel, E.P., Domnanich, K., Clause, H.K., Kalman, C., Walker, W., Shusterman, J.A., Greene, J., Gott, M., Severin, G.W., 2020. Production, Collection, and Purification of ^{47}Ca for the Generation of ^{47}Sc through Isotope Harvesting at the National Superconducting Cyclotron Laboratory. *ACS Omega* 5, 27864–27872. <https://doi.org/10.1021/acsomega.0c03020>
- Ansari, S.A., Pathak, P., Mohapatra, P.K., Manchanda, V.K., 2012. Chemistry of Diglycolamides: Promising Extractants for Actinide Partitioning. *Chem. Rev.* 112, 1751–1772. <https://doi.org/10.1021/cr200002f>
- Ayranov, M., Schumann, D., 2010. Preparation of ^{26}Al , ^{59}Ni , ^{44}Ti , ^{53}Mn and ^{60}Fe from a proton irradiated copper beam dump. *Journal of Radioanalytical and Nuclear Chemistry* 286, 649–654. <https://doi.org/10.1007/s10967-010-0732-0>
- Baimukhanova, A., Radchenko, V., Kozempel, J., Marinova, A., Brown, V., Karandashev, V., Karaivanov, D., Schaffer, P., Filosofov, D., 2018. Utilization of (p, 4n) reaction for ^{86}Zr production with medium energy protons and development of a $^{86}\text{Zr} \rightarrow ^{86}\text{Y}$ radionuclide generator. *J Radioanal Nucl Chem* 316, 191–199. <https://doi.org/10.1007/s10967-018-5730-7>
- Banda, R., Lee, H.Y., Lee, M.S., 2013. Separation of Zr from Hf in acidic chloride solutions by using TOPO and its mixture with other extractants. *J Radioanal Nucl Chem* 298, 259–264. <https://doi.org/10.1007/s10967-012-2349-y>
- Basu, S.K., Mccutchan, E.A., 2020. Nuclear Data Sheets for A = 90. *Nuclear Data Sheets* 165, 1–329. <https://doi.org/10.1016/j.nds.2020.04.001>
- Biswas, S., Basu, S., 1999. Extraction of zirconium(IV) from hydrochloric acid solutions by tri-octylamine and neutral donors. *Journal of Radioanalytical and Nuclear Chemistry* 242, 253–258. <https://doi.org/10.1007/bf02345549>
- Camagong, C.T., Honjo, T., 2001. Separation of Gold (III) as Its Ion-pair Complex with 18-Crown-6 from Hydrochloric Acid Media by Means of Solvent Extraction. *Analytical Sciences* 4.
- Connick, R.E., McVey, W.H., 1949. The Aqueous Chemistry of Zirconium. *J. Am. Chem. Soc.* 71, 3182–3191. <https://doi.org/10.1021/ja01177a070>
- Deri, M.A., Zeglis, B.M., Francesconi, L.C., Lewis, J.S., 2013. PET imaging with ^{89}Zr : From radiochemistry to the clinic. *Nuclear Medicine and Biology* 40, 3–14. <https://doi.org/10.1016/j.nucmedbio.2012.08.004>
- Despotopoulos, J.D., Kmak, K.N., 2021. Rapid isolation of $^{197}\text{m,gHg}$ from proton irradiated Au foils. *J Radioanal Nucl Chem* 327, 1349–1354. <https://doi.org/10.1007/s10967-021-07609-y>
- Dewell, E., Voight, A., 1951. Zirconium ions in aqueous solution (Ames Laboratory ISC Technical Reports).
- Domnanich, K.A., Abel, E.P., Clause, H.K., Kalman, C., Walker, W., Severin, G.W., 2020a. An isotope harvesting beam blocker for the National Superconducting Cyclotron Laboratory.

- Nuclear Instruments and Methods in Physics Research Section A: Accelerators, Spectrometers, Detectors and Associated Equipment 959, 163526.
<https://doi.org/10.1016/j.nima.2020.163526>
- Domnanich, K.A., Vyas, C.K., Abel, E.P., Kalman, C., Walker, W., Severin, G.W., 2020b. Harvesting Zn-62 from an aqueous cocktail at the NSCL. *New J. Chem.* 44, 20861–20870. <https://doi.org/10.1039/d0nj04411c>
- Ellis P. Steinberg, 1960. *Radiochemistry of Zirconium and Hafnium*. The National Academies Press, Washington, DC.
- Fritz, J.S., Abbink, J.E., 1962. Cation Exchange Separation of Vanadium from Metal Ions. *Anal. Chem.* 34, 1080–1082. <https://doi.org/10.1021/ac60189a014>
- Hoffman, R.D., Kelley, K., Dietrich, F.S., Bauer, R., Mustafa, M.G., 2006. Modeled Neutron and Charged-Particle Induced Nuclear Reaction Cross Sections for Radiochemistry in the Region of Yttrium, Zirconium, Niobium, and Molybdenum (No. UCRL-TR-222275). Lawrence Livermore National Laboratory (LLNL), Livermore, CA, US.
<https://doi.org/10.2172/898501>
- Horwitz, E., McAlister, D., Bond, A., Jr, R., 2005. Novel Extraction of Chromatographic Resins Based on Tetraalkyldiglycolamides: Characterization and Potential Applications. *Solvent Extr Ion Exch* 23, 319–344. <https://doi.org/10.1081/SEI-200049898>
- Johnson, T.D., Kulp, W.D., 2015. Nuclear Data Sheets for A = 87. *Nuclear Data Sheets* 129, 1–190. <https://doi.org/10.1016/j.nds.2015.09.001>
- Kraus, K.A., Johnson, J.S., 1953. Hydrolytic Polymerization of Zirconium (IV). *J. Am. Chem. Soc.* 75, 5769–5769. <https://doi.org/10.1021/ja01118a535>
- Kraus, K.A., Nelson, F., 8/7. Anion Exchange Elution Curves HCl, in: *A/CONF*, 837. p. 113.
- Loveless, C.S., Marois, B.E., Ferran, S.J., Wilkinson, J.T., Sutherlin, L., Severin, G., Shusterman, J.A., Scielzo, N.D., Stoyer, M.A., Morrissey, D.J., Robertson, J.D., Peaslee, G.F., Lapi, S.E., 2020. Harvesting 48V at the National Superconducting Cyclotron Laboratory. *Applied Radiation and Isotopes* 157, 109023.
<https://doi.org/10.1016/j.apradiso.2019.109023>
- Margerin, V., Murphy, A.St.J., Davinson, T., Dressler, R., Fallis, J., Kankainen, A., Laird, A.M., Lotay, G., Mountford, D.J., Murphy, C.D., Seiffert, C., Schumann, D., Stowasser, T., Stora, T., Wang, C.H.-T., Woods, P.J., 2014. Study of the $Ti^{44}(\alpha,p)V^{47}$ reaction and implications for core collapse supernovae. *Physics Letters B* 731, 358–361.
<https://doi.org/10.1016/j.physletb.2014.03.003>
- Mastren, T., Pen, A., Loveless, S., Marquez, B.V., Bollinger, E., Marois, B., Hubley, N., Brown, K., Morrissey, D.J., Peaslee, G.F., Lapi, S.E., 2015. Harvesting ^{67}Cu from the Collection of a Secondary Beam Cocktail at the National Superconducting Cyclotron Laboratory. *Analytical Chemistry* 87, 10323–10329. <https://doi.org/10.1021/acs.analchem.5b02322>
- Mastren, T., Pen, A., Peaslee, G.F., Wozniak, N., Loveless, S., Essenmacher, S., Sobotka, L.G., Morrissey, D.J., Lapi, S.E., 2014. Feasibility of Isotope Harvesting at a Projectile Fragmentation Facility: ^{67}Cu . *Scientific Reports* 4, 6706.
- McCutchan, E.A., Sonzogni, A.A., 2014. Nuclear Data Sheets for A = 88. *Nuclear Data Sheets* 115, 135–304. <https://doi.org/10.1016/j.nds.2013.12.002>
- Negret, A., Singh, B., 2015. Nuclear Data Sheets for A = 86. *Nuclear Data Sheets* 124, 1–156. <https://doi.org/10.1016/j.nds.2014.12.045>
- Pen, A., Mastren, T., Peaslee, G.F., Petrasky, K., DeYoung, P.A., Morrissey, D.J., Lapi, S.E., 2014. Design and construction of a water target system for harvesting radioisotopes at the National Superconducting Cyclotron Laboratory. *Nuclear Instruments and Methods in Physics Research Section A: Accelerators, Spectrometers, Detectors and Associated Equipment* 747, 62–68. <https://doi.org/10.1016/j.nima.2014.02.010>

- Pourmand, A., Dauphas, N., 2010. Distribution coefficients of 60 elements on TODGA resin: Application to Ca, Lu, Hf, U and Th isotope geochemistry. *Talanta* 81, 741–753. <https://doi.org/10.1016/j.talanta.2010.01.008>
- Reis, V.H., Hanrahan, R.J., Levedahl, W.K., 2016. The Big Science of stockpile stewardship. *Physics Today* 69. <https://doi.org/10.1063/PT.3.3268>
- Saisho, H., 1962. Note on the Solvent Extraction of Some Metals by Tri-*n*-octyl Phosphine Oxide. *BCSJ* 35, 514–515. <https://doi.org/10.1246/bcsj.35.514>
- Schumann, D., Ayrarov, M., Stowasser, T., Gialanella, L., Leva, A. di, Romano, M., Schuermann, D., 2013a. Radiochemical separation of ⁷Be from the cooling water of the neutron spallation source SINQ at PSI. *Radiochimica Acta* 101, 509–514. <https://doi.org/10.1524/ract.2013.2078>
- Schumann, D., Stowasser, T., Dressler, R., Ayrarov, M., 2013b. Possibilities of preparation of exotic radionuclide samples at PSI for scientific investigations. *Radiochimica Acta* 101, 501–508. <https://doi.org/10.1524/ract.2013.2058>
- Shusterman, J.A., Scielzo, N.D., Abel, E.P., Clause, H.K., Dronchi, N.D., Frey, W.D., Gharibyan, N., Hart, J.A., Loveless, C.S., McGuinness, S.R., Sutherlin, L.T., Thomas, K.J., Lapi, S.E., Robertson, J.D., Stoyer, M.A., Norman, E.B., Peaslee, G.F., Severin, G.W., Shaughnessy, D.A., 2021. Aqueous harvesting of ⁸⁸Zr at a radioactive-ion-beam facility for cross-section measurements. *Phys. Rev. C* 103, 024614. <https://doi.org/10.1103/PhysRevC.103.024614>
- Shusterman, J.A., Scielzo, N.D., Thomas, K.J., Norman, E.B., Lapi, S.E., Loveless, C.S., Peters, N.J., Robertson, J.D., Shaughnessy, D.A., Tonchev, A.P., 2019. The surprisingly large neutron capture cross-section of ⁸⁸Zr. *Nature*. <https://doi.org/10.1038/s41586-018-0838-z>
- Singh, B., 2013. Nuclear Data Sheets for A = 89. *Nuclear Data Sheets* 114, 1–208. <https://doi.org/10.1016/j.nds.2013.01.001>
- Singh, B., Chen, J., 2014. Nuclear Data Sheets for A=85. *Nuclear Data Sheets* 116, 1–162. <https://doi.org/10.1016/j.nds.2014.01.001>
- Sonnabend, K., Mohr, P., Zilges, A., Hertenberger, R., Wirth, H.-F., Graw, G., Faestermann, T., 2003. First excited state of the s -process branching nucleus Zr 95. *Phys. Rev. C* 68, 048802. <https://doi.org/10.1103/PhysRevC.68.048802>
- Takeo, N., 2005. Atlas of Eh-pH diagrams. Geological survey of Japan open file report 419, 102.
- Talip, Z., Dressler, R., David, J.C., Vockenhuber, C., Müller Gubler, E., Vögele, A., Strub, E., Vontobel, P., Schumann, D., 2017. Radiochemical Determination of Long-Lived Radionuclides in Proton-Irradiated Heavy-Metal Targets: Part I—Tantalum. *Anal. Chem.* 89, 13541–13549. <https://doi.org/10.1021/acs.analchem.7b03952>
- Talip, Z., Dressler, R., Schacherl, B., David, J.-C., Vockenhuber, C., Schumann, D., 2021. Radiochemical Determination of Long-Lived Radionuclides in Proton-Irradiated Heavy Metal Targets: Part II Tungsten. *Anal. Chem.* 93, 10798–10806. <https://doi.org/10.1021/acs.analchem.1c00640>
- Wang, L.Y., Lee, H.Y., Lee, M.S., 2013. Solvent Extraction of Zirconium and Hafnium from Hydrochloric Acid Solutions Using Acidic Organophosphorus Extractants and Their Mixtures with TOPO. *Mater. Trans.* 54, 1460–1466. <https://doi.org/10.2320/matertrans.M2013150>
- Wang, L.Y., Lee, M.S., 2016. A review on the aqueous chemistry of Zr(IV) and Hf(IV) and their separation by solvent extraction. *Journal of Industrial and Engineering Chemistry* 39, 1–9. <https://doi.org/10.1016/j.jiec.2016.06.004>
- White, J.C., Ross, W.J., 1958. The Use Of Tri-N-Octylphosphine Oxide In The Solvent Extraction Of Zirconium. United States. <https://doi.org/10.2172/4342898>

Appendix: Supporting Materials

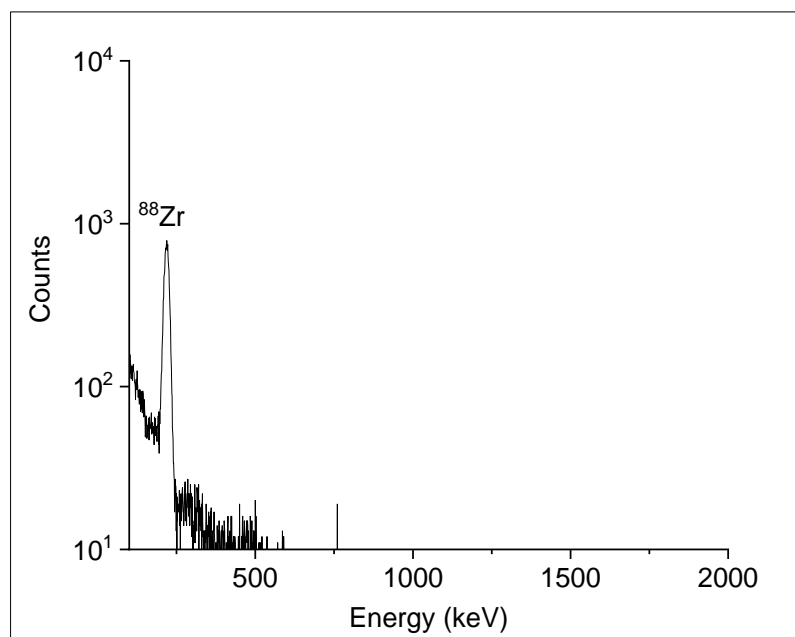


Figure S1: A γ -ray spectrum recorded on a NaI well detector of a 6 M HCl fraction from separation of Al and ^{88}Zr .